NUCLEAR SCIENCE AND ENGINEERING

DOI: https://doi.org/10.1080/00295639.2020.1798728

Th-U Breeding Performances in an Optimized Molten Chloride Salt Fast Reactor

He Liaoyuan,[a,b,c]* Xia Shaopeng,[a,b] Chen Jingen,[a,b,c] Liu Guimin,[a,b,c] Wu Jianhui,[a,b] and Zou Yang[a,b,c]

[a]*Chinese Academy of Sciences, Shanghai Institute of Applied Physics, Shanghai 201800, China*
[b]*Chinese Academy of Sciences, CAS Innovative Academies in TMSR Energy System, Shanghai 201800, China*
[c]*University of Chinese Academy of Sciences, Beijing 100049, China*

Received April 25, 2020
Accepted for Publication July 1, 2020

Abstract — *The molten chloride salt fast reactor (MCFR) with Th-U fuel cycle is attracting more and more attention because of its excellent performance, such as high solubility of actinides, superior breeding capacity, low waste production, and high inherent safety. First of all, the breeding capability of an MCFR at equilibrium state was optimized by an in-house automated optimization program. Based on an optimized MCFR, an investigation of Th-U cycle performance was performed. Due to the lack of available ^{233}U in nature, transuranium (TRU), low-enriched uranium (LEU), and Pu were employed as the startup fissile materials, and two different transition scenarios, a breeding and burning (B&B) scenario and a pre-breeding and burning (PBB) scenario were studied. The results show that the breeding performance in an MCFR is attractive and that the Th-U fuel transition can be achieved smoothly by using LEU, Pu, or TRU as startup fissile materials. In the B&B scenario, the average net ^{233}U production rate in the LEU-started, TRU-started, and Pu-started modes during 200-year operation is 374, 321, and 323 kg/a, respectively, at the reprocessing rate of 200 L/day. While in the PB&B scenario the average annual ^{233}U production is about 570 kg for all startup cases at a reprocessing rate of 40 L/day, and the corresponding doubling time is about 9.6 years. Besides, the values of the fuel Doppler coefficient and density coefficient are negative, and the total temperature coefficient of reactivity in all scenarios is below −8 pcm/K. In addition, the value of radiotoxicity of the Th-U cycle in an MCFR is lower than that in other molten salt reactors like the molten-salt breeder reactor and the molten fluoride salt reactor due to the lower buildup of fission products and TRU under its hard spectrum.*

Keywords — *Th-U cycle, molten chloride salt fast reactor, fast reactor, breeding and burning, pre-breeding and burning.*

Note — *Some figures may be in color only in the electronic version.*

I. INTRODUCTION

The molten salt reactor (MSR) was selected as one of six candidate reactors by the Generation-IV International Forum thanks to its outstanding features on inherent safety, neutron economics, reliability, and proliferation resistance, etc.[1] It is the only liquid fuel reactor in which the fuel salt in the primary loop serves as both fuel and coolant, which means that fuel fabrication is not needed and online fuel reprocessing can be implemented without shutdown of the reactor.[2]

The MSR can use fluoride salt or chloride salt as the fuel carrier, corresponding to two reactor types, i.e., molten fluoride salt reactor (MFSR) and molten chloride salt fast reactor (MCFR). Due to the high corrosiveness of chloride salt and the successful operating experience of

*E-mail: heliaoyuan@sinap.ac.cn

the MFSR, most pioneering studies were focused on the MFSR (Ref. 3 through 6). However, considering the several advantages of chloride salt, it is worth assessing the concept of the MCFR (Ref. 7). First, the energy spectrum is much harder in an MCFR than in a MFSR due to the larger atomic mass of Cl, which leads to a smaller neutron slowing-down ratio and brings great advantages to the breeding performance of fissionable nuclides. In addition, the extraction period of fission products (FPs) can be prolonged owing to their much smaller neutron absorption cross sections in an MCFR. More importantly, chloride salt has a high solubility of actinides, hence a great deal of heavy nuclides can be loaded in the core, which further contributes to the breeding performance and transmutation capacity of an MCFR.

Research on the chloride salt reactor began in the 1950s by Oak Ridge National Laboratory (ORNL), and a MCFR concept was proposed that uses NaCl + $MgCl_2$ + $PuCl_3$ + UCl_3 as fissile fuel salt and UO_2 + Na as solid blanket.[7] The breeding ratio (BR) can achieve 1.09, which mainly demonstrates the feasibility of fuel breeding in a chlorine salt fast reactor. In the 1960s, the British Atomic Energy Authority also carried out research on an MCFR (Ref. 8) in which NaCl + $^{238}UCl_3$ + $PuCl_3$ was used as the driving fuel salt and NaCl + $^{238}UCl_3$ as the breeding fuel salt. With this fuel configuration, the BR can achieve as high as 1.53, which demonstrates a much better fuel breeding capacity than the version designed by ORNL. Currently, there is increasing interest in research on the MCFR around the world. France and Germany have proposed two MCFR concepts, the REBUS (Ref. 9) and the Dual Fluid Reactor[10] (DFR), respectively. REBUS operates at the nominal power of 3700 MW(thermal) in a closed U-Pu cycle and is supposed to be the main component of its future reactor fleet. It shows a rare combination of the following attractive characteristics: a positive breeding gain and a strong negative temperature coefficient of reactivity (TCR). These two features are associated with a simple reactor design and fuel cycle scheme that allows it to meet requirements the address future nuclear systems in full measure. The dual fluid reactor (DFR) combines the advantages of the molten salt reactor experiment (MSRE), the LRF, and the very high temperature reactor (VHTR) by using two separate fluids. The molten salt of the DFR is cooled with a separate liquid lead loop, which allows for higher power densities and better breeding performance. In addition, Moltex Energy in Great Britain[11] has proposed the concept of a stable salt fast reactor that is a pool-type fast reactor in which the fuel tube is loaded with chloride fuel. The stable salt fast reactor has an enormous economic advantage over other fast reactor designs due to its far superior intrinsic safety. It can be both highly profitable at electricity prices lower than those achievable by fossil fuels and clean up the long-lived radioactive waste from current and future generations of light-water reactors (LWRS) simultaneously. However, because most of the above research has been about the U-Pu fuel breeding performance of the MCFR, there has been a lack of attention to the Th-U fuel cycle in the MCFR. Compared with the U-Pu cycle, the Th-U cycle can offer some special advantages. The lower mass number of Th fosters a lower endogenous generation of transuranium (TRU), with the lower TRU buildup in a closed fuel cycle yielding a fuel inventory with lower radiotoxicity and heat load, which benefits public acceptance and repository thermal performance. Besides, Th is more abundant than U in nature, and furthermore, Th use is known to foster improved safety parameters.[4] Thus, it is of great significance to study the Th-U cycle performance in the MCFR.

In 2011, the Strategic Project "Future Advanced Nuclear Energy–Thorium-based Molten Salt Reactor System (TMSR)" was launched by the Chinese Academy of Sciences with the aim to solve the key technical issues of the TMSR and realize the efficient utilization of thorium.[12] Studies have been carried out to assess approaches to thorium fuel utilization for various MSRs, including fuel breeding in a FLiNaK MSFR Ref. 13), an improved molten salt fast reactor,[14] a single-fluid double-zone thorium molten salt reactor,[15] and small modular molten salt reactor.[16] However, there are relatively few studies on the Th-U cycle characteristics of the MCFR. The aim of our work is to investigate the Th-U cycle performance in an optimized MCFR to identify the challenges and limitations for deployment of this reactor.

In order to improve the breeding performance of the MCFR (Refs. 17, 18, and 19), we first optimized the breeding performance of the MCFR in equilibrium state (EQL) by employing a hybrid adaptive intelligent algorithm that combines the genetic algorithm and simulated annealing algorithm.[20] Then, based on the optimized MCFR, low-enriched uranium (LEU), Pu, and TRU were used as startup fuels for thorium fuel cycle transition in the breeding and burning (B&B) and pre-breeding and burning (PB&B) scenarios that were investigated.[21] The characteristics of transition and EQL of these scenarios in terms of the evolution of heavy nuclei, overall breeding capabilities, deterministic safety parameters, waste production, and radiotoxicity level were analyzed.

The description of the reprocessing schemes and calculation tool are introduced in Sec. II. The optimization of the MCFR is discussed in detail in Sec. III. Moreover, Sec. IV analyzes the Th-U cycle performance in the B&B and PB&B scenarios. Conclusions are given in Sec. V.

II. GENERAL DESCRIPTION OF MCFR AND ANALYSIS METHODOLOGY

II.A. Reprocessing Schemes

The reprocessing diagram shown in Fig. 1 refers to the MSFR (Refs. 22 and 23). There are two key processes for the extracting system. The first is the He gaseous bubbling system, which extracts the noble gaseous and metallic FPs (H, He, N, O, Ne, Ar, Kr, Xe, Rn, Zr, Ga, Ge, As, Nb, Mo, Tc, Ru, Rh, Pd, Ag, Cd, In, Sn, and Sb) continuously online. The second is the online chemical reprocessing system that removes soluble FPs using fluorination and reductive extraction techniques. Fluorination is used to remove the elements in gaseous forms in which U, Np, and Pu are extracted first and returned to the core. The reductive extraction step aims to separate most actinides. including Th, Pa, and minor actinides (MA), from the fuel salt and store them in stockpile for several months to let ^{233}Pa decay into ^{233}U. Finally, the carrier salt is recovered by reduced pressure distillation for further utilization.[6]

II.B. Calculation Tool

In this study, the in-house program TMCBurnup, which couples TRITON in the SCALE6.1 program and a depletion program MODEC, was used for burnup calculation. SCALE6.1 is a comprehensive code package developed by ORNL that can be used for the analysis of criticality safety, radiation shielding, radioactive source term, sensitivity, uncertainty, and so on.[24] In this work, TRITON serves as the problem-dependent cross-section processing and multigroup neutron transport calculation.

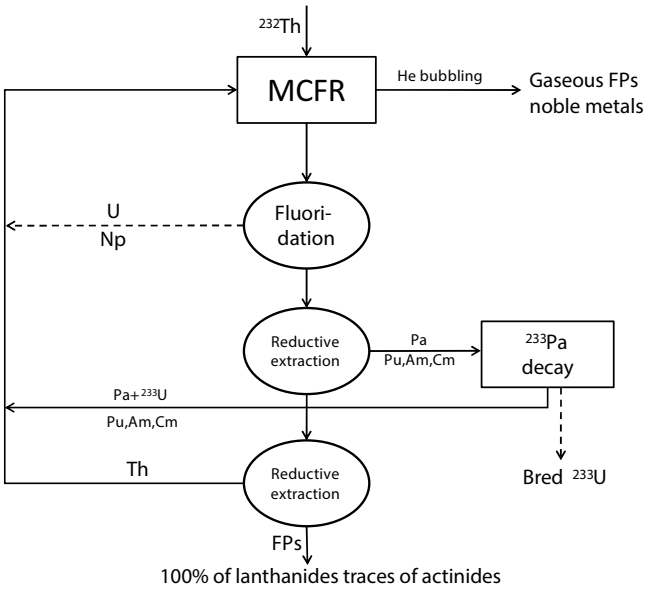

Fig. 1. Reprocessing diagram of an MCFR.

Due to online reprocessing and refueling of the MSR, the depletion equation can be described by improving the conventional depletion equation:

$$\begin{cases} \frac{dNi(t)}{dt} = \sum_j \lambda_{j,i} N_j(t) - \lambda_i N_i(t) + Ci \\ \lambda_{j,i} = f_{j\to i}\sigma_j\phi(t) + \gamma_{j\to i}\lambda_j,\ \lambda_i = \sigma_i\phi(t) + \lambda_i^c \end{cases} \quad (1)$$

where

$N_i(t)$, $N_j(t)$ = number density of nuclide i and j, respectively

$\gamma_{j\to i}$ = branching ratio of decay from nuclide j into i

$f_{j\to i}$ = probability of nuclide j to i by a neutron absorption reaction

λ_i, λ_j = decay constant of nuclide i and j

λ_i^c = fictive decay constant of nuclide i due to chemical reprocessing

σ_i, σ_j = absorption cross sections of nuclide i and j

C_i = feed rate of nuclide i.

In order to solve this nonhomogeneous equation, an in-house MOlten salt reactor specific DEpletion Code (MODEC) was developed in our previous work. MODEC has a strong capability for accurately tracking the evolution of isotopes within and outside of the core to ensure the accuracy of calculation.[25] Besides, to solve the depletion equation two depletion algorithms are embedded: the transmutation trajectory analysis and the Chebyshev rational approximation method. In addition, the fictive decay constant method is applied to simulate the online reprocessing. Compared with ORIGEN-S, the validity of the performance of MODEC in burnup calculations with online reprocessing and continuously refueling is proved.[25]

The flowchart of TMCBurnup is shown in Fig. 2. First, the parameters of the molten salts and the core geometry are input for initialization. Second, the neutron transportation and depletion with online reprocessing and continuous refueling are calculated by the TRITON and MODEC modules, respectively. Third, the ^{233}U and Th are injected into the molten salt to keep the total inventory of heavy nuclides constant while their molar ratio is adjusted automatically as required to maintain the criticality of the core.

In this work, the effective multiplication factor k_{eff} is set at 1.000 to 1.005 during the entire lifespan. Besides, continuous boundary conditions are adopted between the material of the fuel salt, the alloy, the fertile salt, graphite, and B_4C.

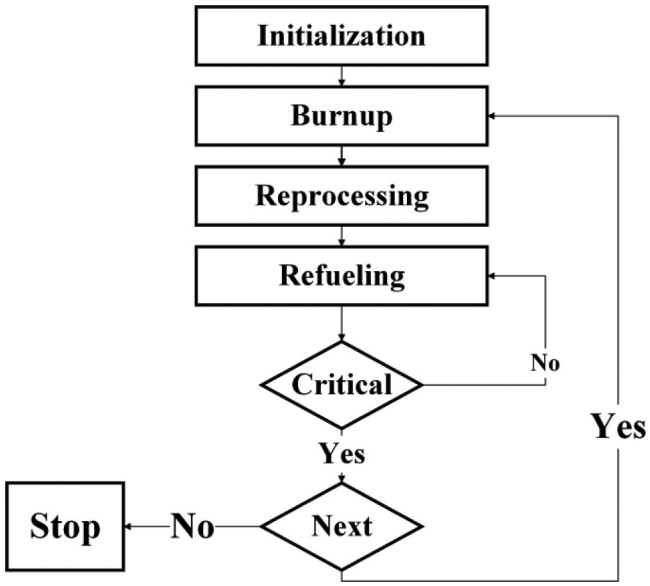

Fig. 2. Flowchart of TMCBurnup.

In order to prove the accuracy of TMCBurnup in the fast reactor calculation, the nuclide evolution of the MSFR was calculated with different startup materials and compared with Ref. 3. The results are shown in Fig. 3. It can be found that the heavy nuclide evolution of TMCBurnup is in good agreement with the reference, which proves the reliability of TMCBurnup in the MSFR calculation. Thus, it is applied for analyzing the Th-U cycle performance of the MCFR.

III. OPTIMIZATION OF THE MCFR

The basic MCFR design in this study, which refers to REBUS-3700, is shown in Fig. 4 (Ref. 9). There are two molten salt zones in the MCFR, i.e., the active zone and the fertile zone. The active core is a compact cylinder (height/diameter ratio = 1.0) where the fuel salt flows from the bottom to the top. The fertile zone, which surrounds the active core in both the radial and axial directions (blue area in Fig. 4), is separated from the fuel zone by a Ti-based alloy. Surrounding the fertile salt is the graphite reflector (yellow area in Fig. 4) that is applied for fertile fuel saving.[26] Outside the graphite reflector, B_4C (green area in Fig. 4) is used for the absorption of the neutrons leaking from the reactor. The composition of the adopted fuel salt and fertile salt is 55 mol % NaCl-45 mol % $(HN)Cl_4$ with a density of 3.6 g/cm^3 (Ref. 27).

Before researching the Th-U cycle performance in the MCFR, the breeding capability of the MCFR at EQL was optimized by a MATLAB script; the flowchart of the script is shown in Fig. 5. The SCALE program is coupled to perform critical calculation. Based on the calculation results the proportion of feeding nuclides will be adjusted automatically to maintain core criticality during operation. The Molten salt reactor Equilibrium-State Analysis code (MESA) is an in-house program that was used to quickly obtain the EQL of the MSR (Ref. 28). Besides, in the optimization module, a novel hybrid adaptive intelligent algorithm was developed in-house and applied to improve the optimization capability.[20] The algorithm couples the global search ability of the genetic algorithm and the ability to jump out of a local optimal solution of simulated annealing. Moreover, the adaptive genetic operators, which can change automatically during the optimization, were embedded to improve the quality of the algorithm. The flowchart of the algorithm is shown in Fig. 5, which has been proven to have good performance in handling multiobjective optimization.[20]

In the optimization, nine independent variables (including the core volume, the thickness of blanket, etc.) that had been tested for an obvious impact on the breeding capability

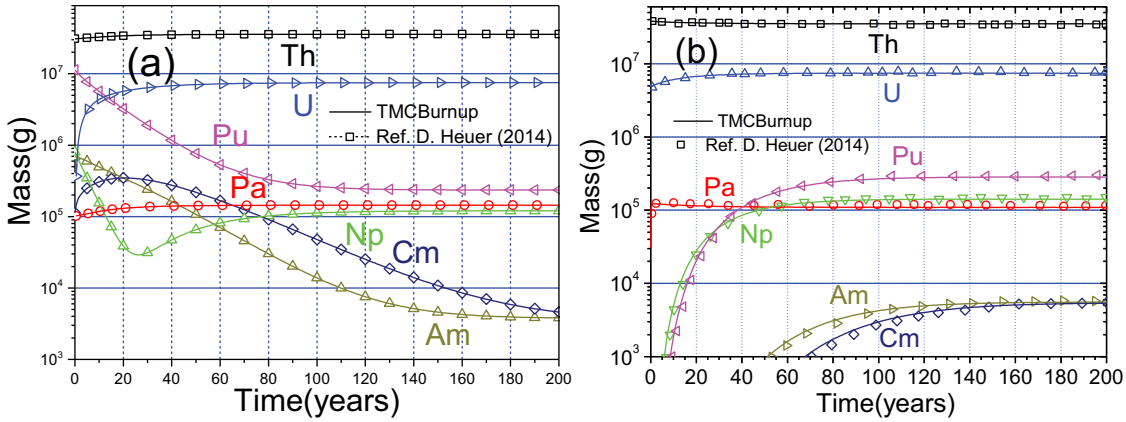

Fig. 3. Evolution of heavy nuclides for the MSFR started with (a) TRU and (b) ^{233}U.

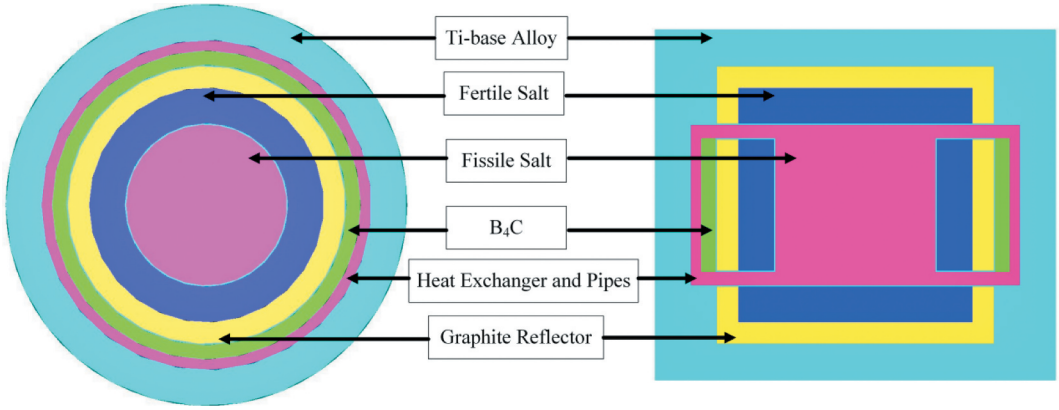

Fig. 4. Cross and vertical sections of an MCFR.

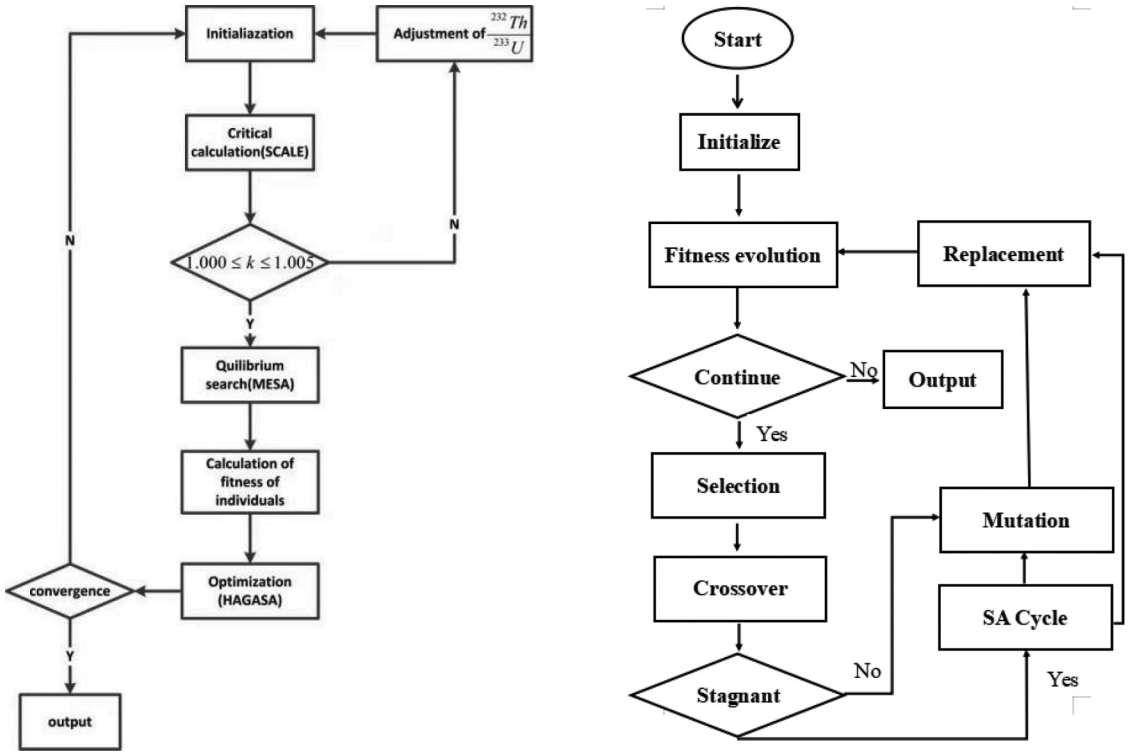

Fig. 5. Flowchart of the optimization of an MCFR and Hybrid Adaptive Genetic Algorithm and Simulation Annealing (HAGASA).

of the MCFR were optimized simultaneously to achieve the best breeding performance at EQL. The value of some important parameters, including the nine optimized variables of the MCFR are listed in Table I.

IV. THORIUM-URANIUM BREEDING PERFORMANCES OF THE OPTIMIZED MCFR

The primary objective of this research is to evaluate the Th-U cycle performance of an optimized MCFR in two different transition modes. However, thanks to the fact that there is no available ^{233}U in nature, it is necessary to investigate the Th-U fuel breeding capability with Pu, TRU, or LEU as starting fuels. In this paper, we analyze three starting fuels depicted as follows:

1. 19.75% LEU as starting fuel
2. TRU produced in LWRs as initial fissile material
3. plutonium fuel produced in LWRs as startup fuel to start the MCFR.

For the LEU-started mode, the enrichment of ^{235}U is set to 19.75% to prevent nuclear proliferation. The Pu-started

TABLE I

Main Parameters of the MCFR

Parameter[a]	Value
Volume of core (m^3)	25.00
Thickness of blanket (radial) (cm)	80
Thickness of blanket (axial) (cm)	60
Thickness of graphite (radial) (cm)	60
Thickness of graphite (axial) (cm)	45
Extraction rate of ^{233}Pa (core) (L/day)	120
Extraction rate of ^{233}Pa (blanket) (L/day)	200
Removal rate of FPs (core) (L/day)	90
Removal rate of FPs (blanket) (L/day)	40
Thermal expansion (K^{-1})	−3.00E−4
Enrichment of ^{37}Cl (%)	97
Temperature of fuel salt (K)	923
Temperature of fertile salt (K)	873
Density of molten salt ($g \cdot cm^3$)	3.6
Density of alloy ($g \cdot cm^3$)	8.86
Density of B_4C ($g \cdot cm^3$)	2.52

[a]The first nine parameters are the optimized variables the MCFR.

mode appears more practical today since it would employ the current PUREX reprocessing technique and facilities to recover Pu from LWRs (Ref. 29). Moreover, the entire TRU vector from LWRs could also be the startup fuel. In this case, five-year-cooled TRUs from LWR used fuel are applied.[30] The initial nuclei inventories of the MCFR with these starting fuels are detailed in Table II. (In these initial nuclei inventories, the MCFR can be critical.) For comparison, the ^{233}U-started case is also listed in Table II. The required initial fissile fuel inventory in the LEU-started case is maximum due to the inferior fission property of ^{235}U under the fast spectrum.

IV.A. Thorium Fuel Cycle Transition for the B&B Scenario

In the B&B scenario, ^{233}U produced from the decay of the extracted ^{233}Pa needs to be fueled back to the reactor to maintain criticality. In this subsection, we analyze the characteristics of the Th-U cycle of the MCFR in the B&B

TABLE II

Initial Nuclei Inventories of an MCFR with Different Starting Fuel*

Nuclide	Pu Started	TRU Started	LEU Started	^{233}U Started
^{232}Th	1.78E+05	1.75E+05	5.09E+04	1.92E+05
^{233}U				2.36E+04
^{235}U			3.27E+04	
^{238}U			1.30E+05	
^{237}Np		2.46E+03		
^{238}Pu	7.42E+02	8.07E+02		
^{239}Pu	2.15E+04	1.80E+04		
^{240}Pu	1.04E+04	8.44E+03		
^{241}Pu	1.48E+03	4.20E+03		
^{242}Pu	2.97E+03	2.63E+03		
^{241}Am		1.34E+03		
^{243}Am		7.47E+02		
^{244}Cm		3.14E+02		
^{245}Cm		3.93E+01		

*Unit = mole.

scenario in terms of deterministic safety parameters, breeding capability, neutron spectra, and radiotoxicity evolution. A 238-group ENDF-B/VII.0 cross-section library was used in the calculation. In addition, there were 10 000 neutrons per k_{eff} cycle. We skipped the first 15 k_{eff} cycles to allow the spatial fission source to attain equilibrium before the k_{eff} values were used to average the final k_{eff} estimate. A total of 285 k_{eff} cycles were run in a criticality calculation with an average error of about 25 pcm.

IV.A.1. Comparison of Neutron Spectra

Neutron spectra that could help fundamentally indicate subsequent interpretations of results based on the actinide buildup and the total TCR are researched here. The neutron spectra of the MCFR at initial and EQL are shown in Fig. 6. Figure 6 shows that there is almost no difference in neutron spectra with the three different startup fuels at the initial state. In order to present a quantitative description for the neutron spectra, the energy of the average lethargy-causing fission (EALF) is introduced,[31] which can be expressed as

$$\mathrm{EALF} = \exp\left\{\frac{\int(\ln E)\phi(E)\sum_f(E)dE}{\int\phi(E)\sum_f(E)dE}\right\}, \qquad (2)$$

where $\phi(E)$ and $\Sigma_f(E)$ represent the energy-dependent neutron-flux and macroscopic fission cross section, respectively. The higher the value of EALF, the harder the neutron spectrum. The evolution of EALF is shown in Fig. 6. It can be found that the EALF of the LEU-started mode increases quickly in the first few years due to the decrease of ^{238}U, and that it has a broader resonance peak and a larger resonance capture cross section than ^{232}Th, resulting in a more obvious resonance in the neutron spectra. Then, it gradually drops to an EQL thanks to the buildup of FPs, which leads to the moderation of neutrons in the fast neutron spectra. In addition, the EALF of the TRU-started and Pu-started modes can transition to EQL more quickly and smoothly thanks to the rapid fuel transition.

IV.A.2. Evolution of Heavy Nuclides

The evolution of heavy nuclides, which are presented in Figs. 7a and 7b, provides an important basis for the analysis of core critical performance and nuclear waste production. Due to the fact that the Pu-started and TRU-started modes have a similar nuclide evolution trend, only the heavy nuclide evolution of the LEU-started and Pu-started modes are displayed. In general, compared to the MSFR some heavy nuclides in the MCFR, especially MAs, need to take a much longer time to achieve equilibrium due to their lower specific power. Besides, the isotopes of Th, Np, Pa, and U reach the EQL more quickly than the other heavy nuclides. In addition, the time for the in-core MAs, like Cm inventory, to reach a maximum in the Pu-started mode is shorter than in the LEU-started mode, which is clearly related to the fact that more neutron captures are necessary to generate MA isotopes in the LEU-started mode than in the Pu-started mode. Moreover, in the LEU-started mode it is time consuming to burn off all ^{238}U, which on the one hand reduces ^{233}U production thanks to the loss of neutrons capture by ^{238}U, but on the other hand delays the time for the nuclide to reach equilibrium. Furthermore, it should

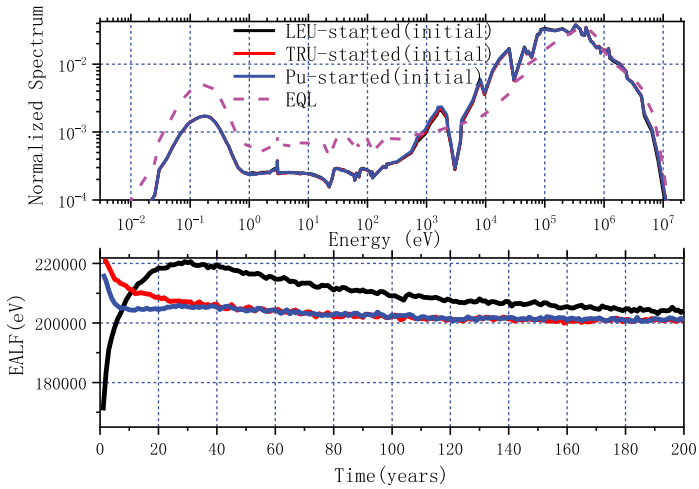

Fig. 6. Neutron spectra and the evolution of EALF of all startup cases.

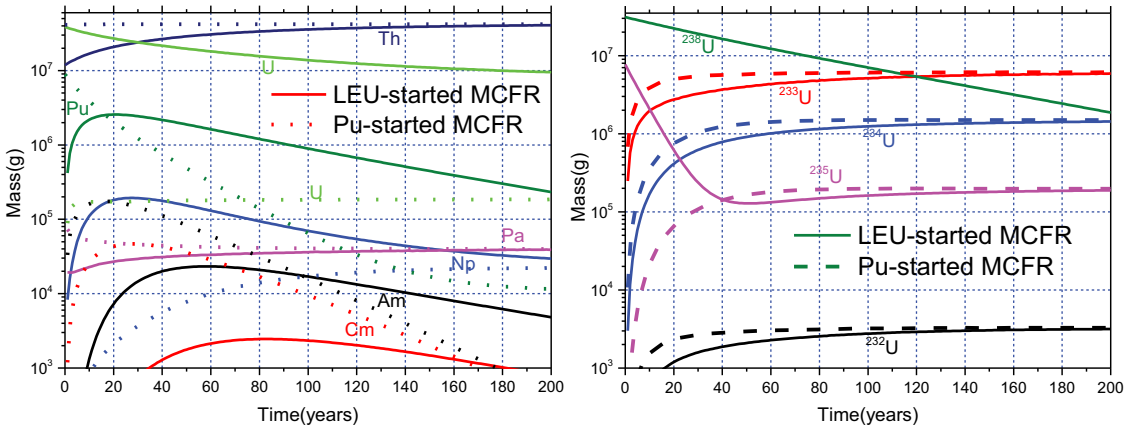

Fig. 7. (a) Evolution of heavy nuclides and (b) uranium isotopes.

also be pointed out that during the whole operation, the content of ^{232}U of the Pu-started mode is always higher than that of the LEU-started mode. This is because the generation of ^{232}U mainly relies on the (n, $2n$) reaction of ^{233}U (Ref. 31). Its reaction cross section increases with the hardening of the neutron spectrum, while the neutron spectrum of the Pu-started MCFR is harder than the LEU-started mode (as shown in Sec. IV.A.1). The ^{232}U decay chain has extremely strong radioactivity, especially from ^{228}Th to ^{208}Tl, and the intensity of the emitted gamma rays is up to2.615 MeV, which greatly increases the nuclear proliferation-resistance capability in the Pu-started mode.

The U isotopes of the blanket are shown in Fig. 8, which indicates that the purity of ^{233}U is pretty high, with the content almost 95.28% thanks to the low content of ^{234}U (1%), and more importantly, ^{232}U (6 ppm). Thus nuclear proliferation-resistance issues arise because it is easy to retrieve ^{233}U from the blanket though a fluorination process.

IV.A.3. Uranium-233 Breeding Capability with Different Starting Fuels

In this subsection, breeding performance with different starting fuels is explored from the aspects of BR, net production of ^{233}U, and doubling time (DT), which are three important parameters for evaluating the breeding performance of an MSR. The BR represents the ratio of the capture rates of all fertile isotopes to the absorption rate of all fissile isotopes, which is defined in Eq. (3):

$$BR = \frac{Rc(^{234}U + ^{232}Th + ^{240}Pu + ^{238}U) - Ra(^{233}Pa)}{Ra(^{233}U + ^{235}U + ^{241}Pu + ^{239}Pu)} \quad (3)$$

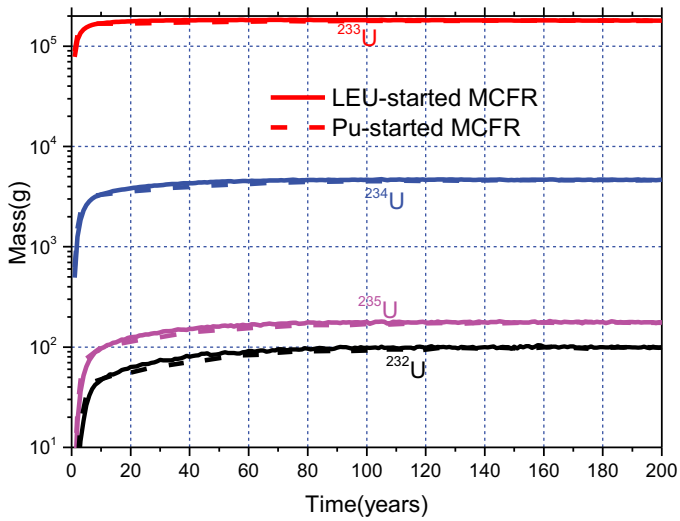

Fig. 8. Evolution of uranium isotopes in blanket.

The evolution of the BR and k_{eff} during the whole operation time is shown in Fig. 9. It can be found that the k_{eff} is between 1.000 and 1.005 during the whole operation, while the BR increases gradually in the LEU-started mode in the first few decades and then reaches an equilibrium state. However, in the Pu-started and TRU-started modes, the BR decreases gradually at the beginning. This is because ^{233}U plays a gradually dominating role in maintaining criticality with the burnup. Its effective fission neutron number under the fast spectrum is larger than ^{235}U and smaller than ^{239}Pu. Moreover, due to the fact that ^{233}U and ^{232}Th are refueled online, the nuclide composition tends to be similar in those three modes, which results in the final BRs of these three startup modes tending to be the same.

In the MSR, the net ^{233}U production is the difference in mass between the extracted ^{233}Pa and the refueled ^{233}U. When the net production of ^{233}U equals the initial inventory of ^{233}U, it is sufficient to start a new MCFR, and the corresponding time is called DT. For a MCFR, the initial loading mass of ^{233}U is 5.5 tons.

The evolution of net ^{233}U production is shown in Fig. 10. The evolution of net ^{233}U production can be divided into two stages: in the first 8 years, the rate of net ^{233}U production in the Pu-started and TRU-started modes is faster, which is mainly due to the higher ^{238}U content in the LEU-started mode, which reduces ^{233}U production thanks to the loss of neutrons captured by ^{238}U. While in the last 192 years, the rate of net ^{233}U production in the LEU-started mode is faster, and the rate of net ^{233}U production between the three modes is gradually narrowed with burnup.

To explain this phenomenon, the concept of a regeneration ratio (RR) is defined in Eq. (4), which directly reflects the relationship between the production and disappearance rate of ^{233}U (Ref. 32):

$$\mathrm{RR} = \frac{R_c(^{232}\mathrm{Th}) - R_a(^{232}\mathrm{Pa})}{R_a(^{233}\mathrm{U})} \tag{4}$$

The evolution of RR is also shown in Fig. 10, and the corresponding fission rate fraction of fissile nuclides is shown in Fig. 11. It can be found that in the second stage, the fission rate fraction of ^{239}Pu generated by the (n,γ) reaction of ^{238}U in the LEU-started mode is largest. It reduces the consumption of ^{233}U, which leads to the fastest ^{233}U production. With the burnup, the nuclide composition and RR in different modes tend to be consistent, thus the net ^{233}U production rate gradually tends to be the same.

The average net ^{233}U production rate in the LEU-started, TRU-started, and Pu-started modes during the

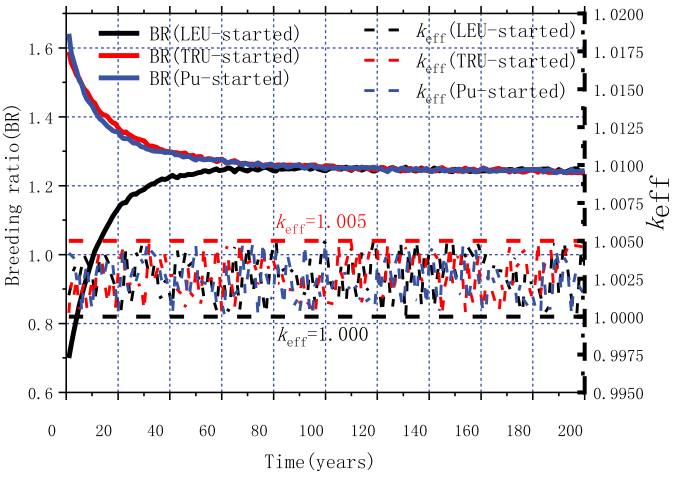

Fig. 9. Evolution of BR and k_{eff}.

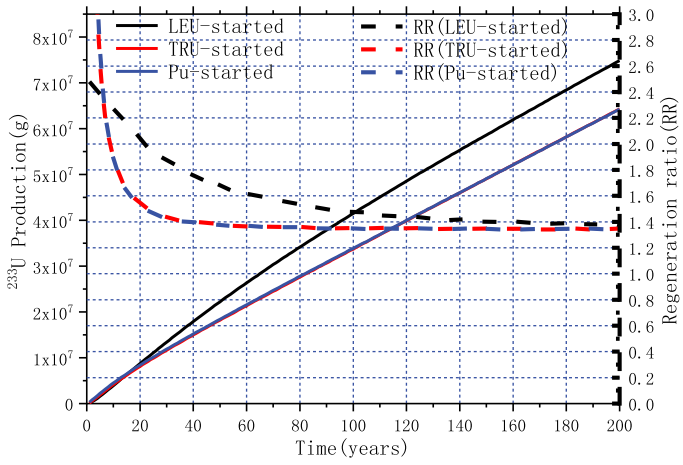

Fig. 10. Evolution of RR and ^{233}U production.

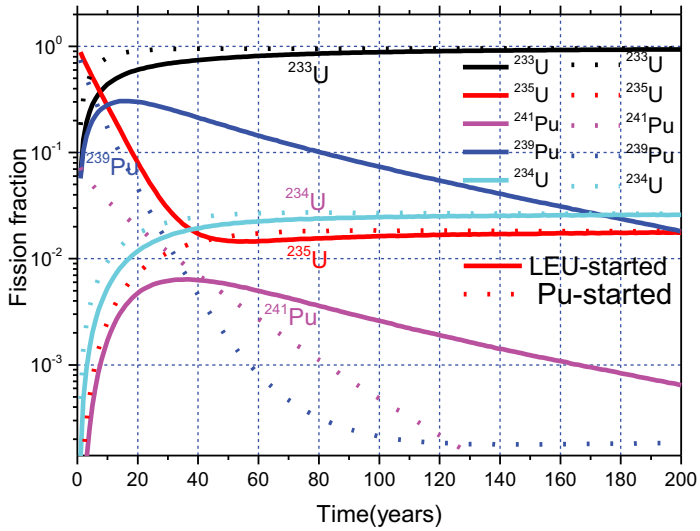

Fig. 11. Evolution of fission fraction.

200-year operation is 374, 321, and 323 kg/a, respectively, and the corresponding DTs are 17.0, 16.5, and 16.5 years, respectively. While the average net ^{233}U production rate at EQL is 274 kg/a for all startup cases, the corresponding DTs are almost equal to 20.1 years at EQL. Besides, the ^{233}U produced in the core is less than the feed during operation at the early stage, and the maximum deficit of ^{233}U corresponding to the LEU, Pu, and TRU startup modes is 102, 87, and 83 kg, respectively.

IV.A.4. Safety Parameter Analysis

In this subsection, two important parameters, TCR and β_{eff} are investigated from the beginning of life to equilibrium. In the MSR, TCR must be negative during the whole operating time to ensure the reactor is intrinsically safe, while the β_{eff} plays an important role in both kinetics reactivity controlling safety and static reactor physics experiments. Safety parameter analysis can provide insight into the MCFR safety performance and the relative potential of the various modes.

Thanks to the fact that there is no moderator in an MCFR, the reactivity feedback coefficient is only affected by the expansion of the salt and the core structures. For an MCFR, the feedback coefficient of the core structure is clearly positive, however, the expansion coefficient of the structures is much lower than the thermal expansion coefficient of the salt.[26] Moreover, during a transient, the fuel salt undergoes obvious and quick temperature variations, while a much smaller and slower temperature change happens to the core structure, and thus, this effect can be ignored. So, the TCR in an MCFR can be defined as

$$\frac{dK}{dT})total = \frac{dK}{dT})\ fuel\ Doppler + \frac{dK}{dT})\ fuel\ density \qquad (5)$$

where K and T represents the k_{eff} and the temperature, respectively. The evolution of the TCR for the three different startup modes is shown in Fig. 12, where it can be found that the constant value of the TCR of the TRU-started mode is smallest at initial state, and the TCRs of the three modes are nearly the same at EQL. In an MSR, the Doppler effect is predominant and is driven by resonance capture in the fertile isotope. The ensuing spectrum shift that increases the fertile captures affects the fission and captures in other isotopes. As the dominant fissile isotope of the TRU-started and Pu-started cases, ^{239}Pu has a flatter fission cross section than ^{233}U and ^{235}U in the energy domain of interest for the MCFR. Thus, spectral hardening has a less negative impact on ^{239}Pu fission rather than on ^{233}U and ^{235}U. Plutonium-239 and uranium-235 also have a steeper capture cross section as compared to ^{233}U, suggesting a higher decrement of captures following spectral hardening, thus positively affecting the TCR. The fuel expansion coefficient is mainly driven by leakages, which depend only mildly on fuel composition. Thus, a high ^{233}U content is beneficial for the TCR. Moreover, FP cross sections generally decrease with neutron energy, hence higher FP content suggests a higher decrement in FP captures with spectrum hardening, which leads to increased reactivity, positively affecting the TCR. Thus, the TCR of the TRU-started mode is smallest at initial time and gradually improves due to the fact that the initial starter ^{239}Pu

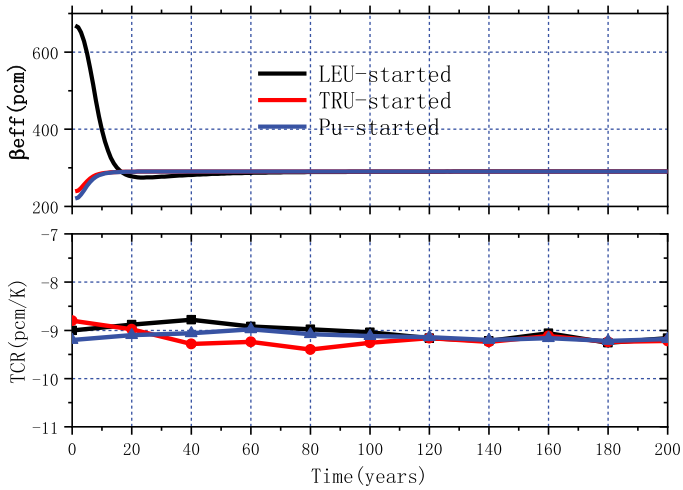

Fig. 12. Evolution of TCR and β_{eff} of all startup cases.

is gradually replaced by ^{233}U with operation. Moreover, though ^{233}U also plays a gradually enhanced role in maintaining criticality with the operation in the Pu-started and LEU-started modes, their TCRs fluctuate very slightly due to the buildup of FPs.

Moreover, β_{eff} is extremely important for reactor operation control, which is primarily determined by the fission rate fraction (see Fig. 11) and the delayed neutron fractions of the single fissionable isotopes (see Table III). It can be expressed as

$$\beta_{eff} = \frac{\sum_i \overline{\nu}_d(i).R_f(i)}{\sum_i \left(\overline{\nu}_d(i) + \overline{\nu}_p(i)\right).R_f(i)} \quad (6)$$

where $\nu d(i)$ and $\nu p(i)$ stand for the average delayed neutrons and the prompt neutrons per fission for nuclide i, respectively, and $Rf(i)$ indicates the fission rate of nuclide i. Due to the high content and a non-negligible fission cross section of ^{234}U in the MCFR energy spectrum, the fission contribution of ^{234}U was also taken into account. The evolution of the total β_{eff} of the different startup modes is displayed in Fig. 12. In the LEU-started mode, the total β_{eff} dropped rapidly in the first few decades, then it increased slightly and gradually transitioned to an EQL. A rapid decline in β_{eff} is primarily due to a decrease in the fission rate fraction of the dominant fissile isotope ^{235}U, while that of other fissile isotopes, especially ^{233}U, increased (Fig. 11). After the first 20 years, with the depletion of ^{239}Pu and the increase of the fission fraction of ^{234}U, the total β_{eff} gradually increased and then tended to be constant. In addition, due to the relatively high delayed neutron fraction, higher ^{241}Pu content is beneficial for β_{eff}, which explains the improved β_{eff} value of the TRU-started mode compared to the Pu-started mode. With the initial starter ^{239}Pu gradually replaced by ^{233}U (see Fig. 11), the β_{eff} gradually increases and then tends to be a constant value of about 291 pcm, which is almost the same as the single delayed neutron fraction of ^{233}U (see Table III). In general, during the whole operation, the value of β_{eff} for the LEU-started, TRU-started, and Pu-started modes changes to 377, 53, and 70 pcm, respectively. Thanks to the dramatic decrease of the β_{eff} corresponding to the LEU-started mode, it may lead to some difficulties in the reactivity control of the MCFR.

IV.A.5. Radiotoxicity and Decay Heat

Radiotoxicity analysis is an important aspect of reactor safety analysis. In this section, the radiotoxicity of the nuclear waste was analyzed to provide relevant parameters for the intermediate storage and final repository of nuclear waste. Due to the fact that an MCFR works in a closed cycle, all the actinides are disposed of only at reactor decommission. Thus, the radiotoxicity and decay heat generated mostly derive from FPs during online reprocessing. Besides, a loss rate of 10^{-5} for TRU and 10^{-7} for uranium isotopes is assumed in our work.[33] These isotopes are also the source of radiotoxicity and decay heat. Figure 13 shows the evolution of radiotoxicity and decay heat of FPs and other loss materials. The horizontal reference line represents the balanced radiotoxicity of natural uranium ore.[34] As can be seen from Fig. 13, FPs are the main source of radiotoxicity and decay heat of material losses during the whole operation. The initial decay heat and radiotoxicity are mainly derived from ^{137}Cs and ^{90}Sr, which have a half-life of about 30 years. As they decay, radiotoxicity and decay heat decrease rapidly, and total radiotoxicity drops below

TABLE III

Delayed Neutron Fraction for Different Isotopes in the MCFR Core

Fission Isotope	^{233}U	^{234}U	^{235}U	^{239}Pu	^{241}Pu
β_{eff} (pcm)	291	531	668	219	543

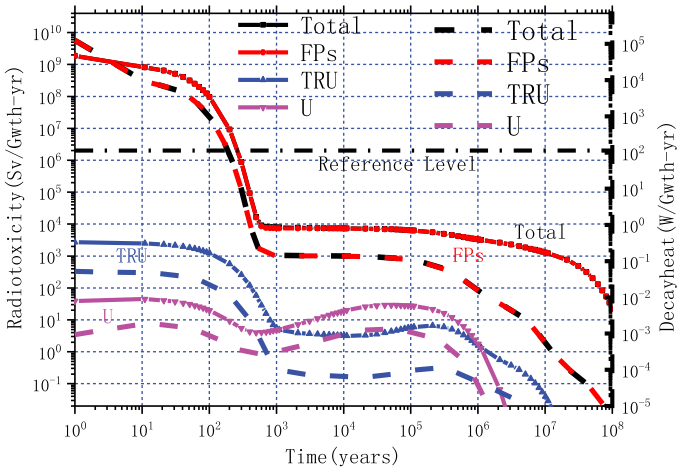

Fig. 13. Evolution of radiotoxicity and decay heat of nuclear waste being lost (the dot and solid line refer to the decay heat and radiotoxicity of the MCFR, respectively).

the reference level in about 300 years. Besides, it can be found that TRU and U isotopes cause a second radiotoxicity and decay heat peak in the long term due to the buildup of the decay products from ^{233}U, ^{234}U, and TRU such as ^{229}Th, ^{225}Ac, and ^{225}Ra. Besides, thanks to the harder spectrum, the content of FPs in an MCFR is lower than in other MSRs, like the MSBR and MSFR, which leads to a lower level of radiotoxicity and decay heat in the MCFR (Refs. 17 and 28).

Because the outer container needs to be replaced during operation, the evolution of radioactivity and decay heat in the reactor is also simulated to provide reference for shielding and fuel storage during the process of container replacement. The evolution of radioactivity and decay heat associated with the equilibrium core inventories and the startup loadings of the TRU-started and Pu-started modes is shown in Fig. 14. It can be observed that the transition from the Th-TRU fuel to the Th-U fuel leads to a notable reduction in short-middle-term radiotoxicity. In addition, thanks to the buildup of the decay products from ^{233}U and ^{234}U, the long-term peak of Th-U fuel will arise. Thus, the choice of an initial TRU loading from LWR-reprocessed fuel overcomes the unavailability of ^{233}U in nature and reduces the decay heat as well as radiotoxicity legacy from LWR operation.

IV.B. Thorium Fuel Cycle Transition for the PB&B Scenario

In the PB&B scenario, the ^{233}U produced from the decay of the extracted ^{233}Pa will build up outside the core. The initial starting fuel and ^{232}Th are fed continuously to maintain the criticality of the core.[35] In the PB&B scenario, TRU, Pu, and LEU, which have the same compositions as in the B&B scenario, are used as both startup fuels and feeding fuels to achieve the purpose of rapid production of ^{233}U. Under the rapid extraction of ^{233}Pa in the core, the LEU-started mode cannot maintain criticality even if pure LEU is fed into the core continuously due to the buildup of FPs and the less number of fission neutrons per absorbed neutron ($\upsilon\Sigma_f/\Sigma_c$) for ^{235}U. With this in mind, the reprocessing rate is set to 40 L/day for the three startup modes.

In the PB&B mode, the production of ^{233}U is achieved by the continuous consumption of the startup fissile materials. Considering the particularity of the PB&B scenario, the concept of replacement ratio (RepR) is introduced, which can be expressed as

$$\mathrm{RepR} = \frac{R_c(^{232}\mathrm{Th}) - R_a(^{233}\mathrm{Pa})}{R_a(^{235}\mathrm{U} + ^{241}\mathrm{Pu} + ^{233}\mathrm{U} + ^{239}\mathrm{Pu})} \quad (7)$$

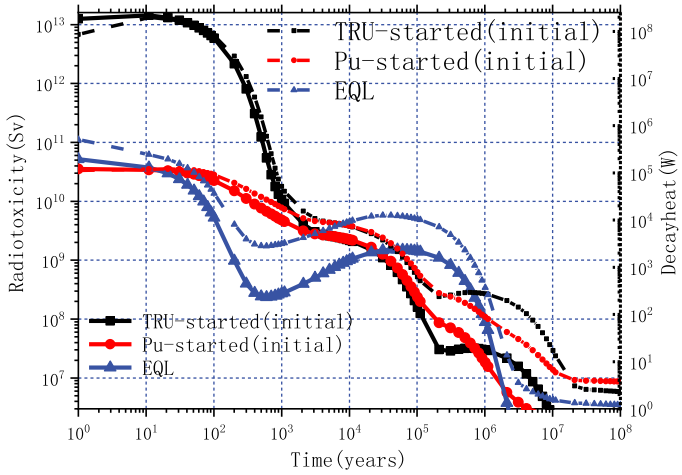

Fig. 14. Evolution of the radioactivity and decay heat at EQL (the dot and solid line refer to decay heat and radiotoxicity, respectively).

where R_a and R_c stand for the absorption and capture rate, respectively, and RepR represents the relationship between the production rate of ^{233}U and the consumption rate of fissile materials. RepR is an important parameter for representing breeding capacity in the PB&B mode. The evolution of the replacement ratio and the k_{eff} of the three cases is shown in Fig. 15. It can be observed that the replacement ratio in the LEU-started mode is lower than the others, even though the RepR gradually increases in the first 60 years. This means that more fissile materials need to be consumed to produce the same amount of ^{233}U in the LEU-started mode than in the other modes.

Moreover, the evolution of the net production of ^{233}U is shown in Fig. 16, which shows that the net production rate of ^{233}U in the three startup modes is almost similar thanks to the too-slow reprocessing rate. In the TRU-started and Pu-started modes, the ^{233}Pa and ^{233}U produced in the core cannot be extracted out of the core in time. Uranium-233 plays a dominate role in rapidly maintaining criticality (see Fig. 17), so the net production of ^{233}U in the TRU-started and Pu-started modes is comparable to that of the LEU-started mode. Under this low core reprocessing rate case, the average net production of ^{233}U for these three startup modes are almost 570 kg/a, and the corresponding DT is about 9.6 years. When the core reprocessing rate increased to 200 L/day, the LEU-started mode could not always maintain criticality during the whole operation, while for the TRU-started and Pu-started modes, the average net production of ^{233}U will increase to 807 and 803 kg/a, and the corresponding DT will decrease to 6.8 years.

In the PB&B mode, the evolution of the TCR is shown in Fig. 18, where it can be seen that the TCRs of the three modes increase rapidly in the first 20 years due to the buildup of FPs. However, the TCRs of all startup modes are below −8.3 pcm/K during the whole operation, which ensures safety with the introduction of positive reactivity. However, in the case of overcooling or fuel salt loading, it is necessary to be careful of the positive reactivity caused by the large negative TCR.

In addition, the evolution of β_{eff} is shown in Fig. 18. The value of β_{eff} in the LEU-started mode decreases from 668 to 369 pcm, while the value of β_{eff} in the Pu-started and TRU-started modes increases from 220 to 286 pcm and 239 to 288 pcm, respectively.

In the PB&B mode, the radiotoxicity and decay heat of material losses during reprocessing and at EQL were also analyzed. Thanks to the different feeding fuel compositions during reactor operation, the nuclide compositions at EQL are different. The content of heavy nuclides and seven important FPs (five long-lived isotopes, namely, ^{79}Se, ^{93}Zr, ^{126}Sn, ^{129}I, and ^{135}Cs and two short-lived isotopes, namely, ^{137}Cs and ^{90}Sr) at EQL are shown in Figs. 19 and 20. It can be seen that the content of TRU in the TRU-started and Pu-started modes is higher than in the LEU-started mode thanks to the fact that the number of neutron captures necessary for U to generate TRU is more than Pu. In addition, the content of FPs in the LEU-started mode is highest due to the softer neutron spectra.

The evolution of radiotoxicity and the decay heat of material losses are shown in Figs. 21 and 22, which show that the value of radiotoxicity and the decay heat of the TRU-started and Pu-started modes is bigger initially due to the higher content of short-lived FPs. Besides, the evolution of radiotoxicity and decay heat at EQL of the core are shown in Fig. 23, where it can be seen that the radiotoxicity

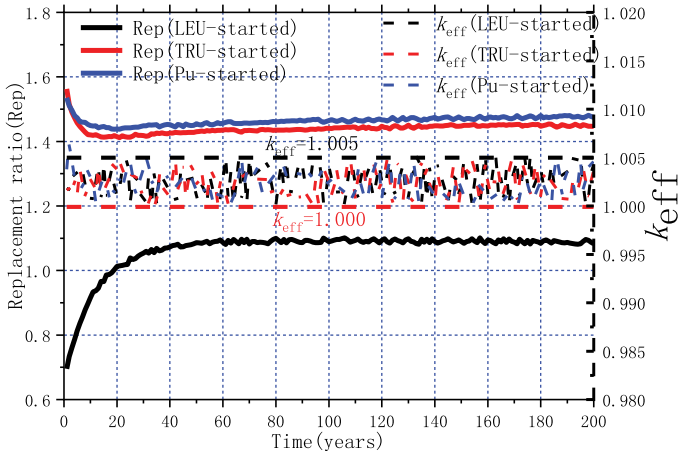

Fig. 15. Evolution of RepR and k_{eff}.

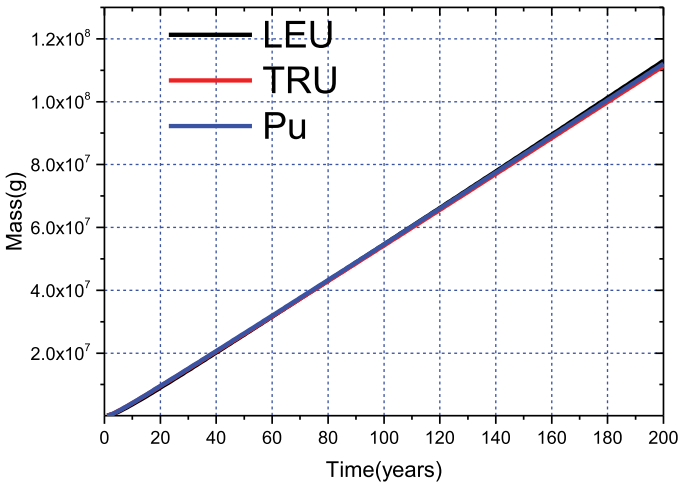

Fig. 16. Evolution of RR and ^{233}U production.

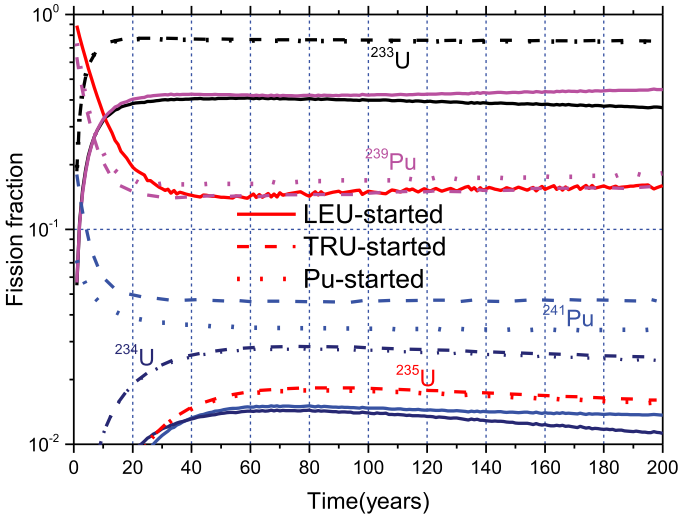

Fig. 17. Evolution of fission fraction of all startup cases.

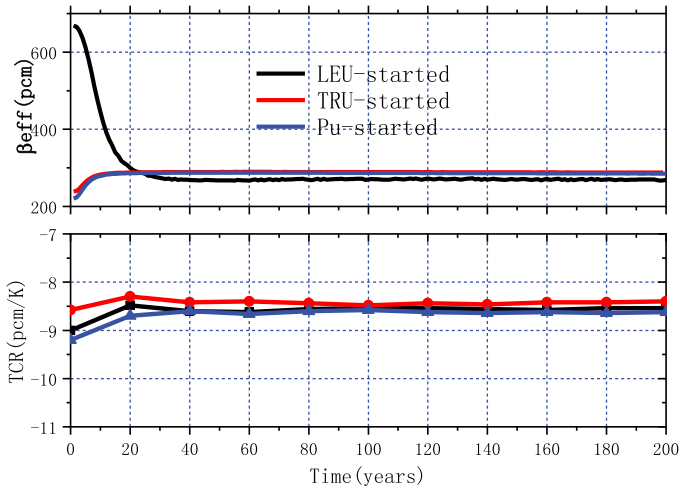

Fig. 18. Evolution of TCR and β_{eff} of all startup cases.

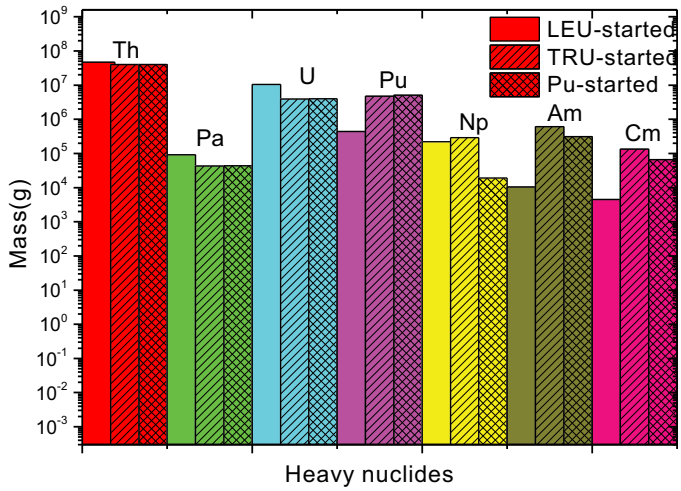

Fig. 19. Heavy nuclides in EQL.

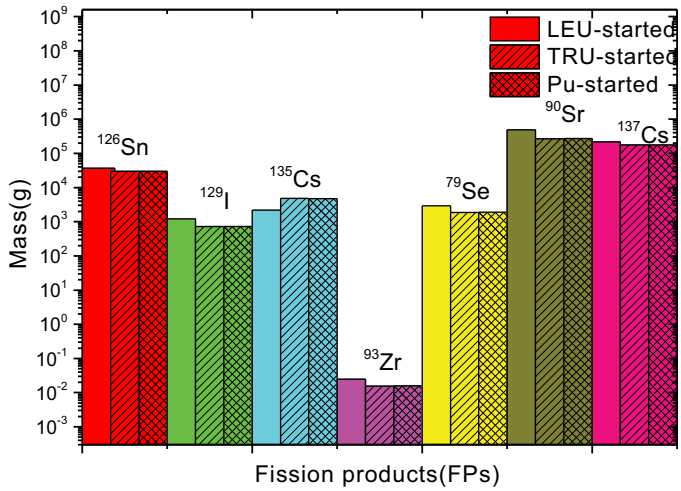

Fig. 20. Fission products in EQL.

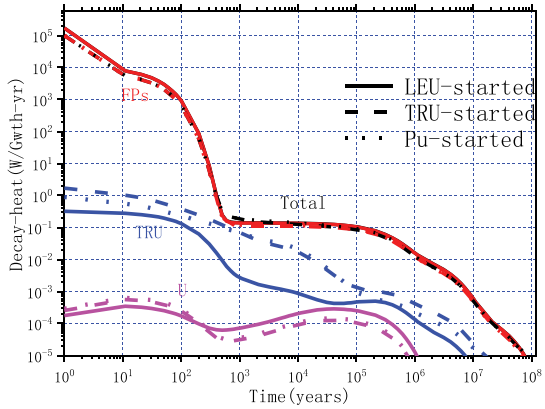

Fig. 21. Evolution of decay heat.

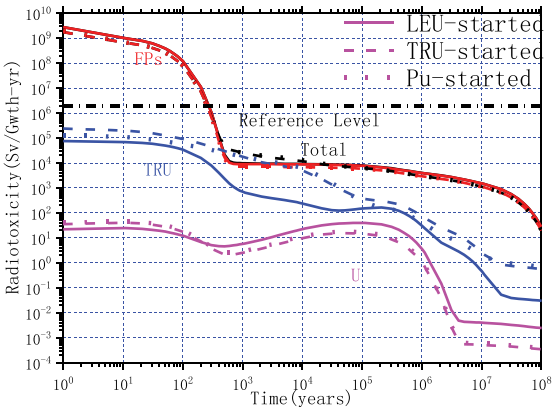

Fig. 22. Evolution of radiotoxicity.

and decay heat in the TRU-started mode is highest during the first 1000 years, which is mainly derived from the highest content of TRU. Only the LEU-started mode inherits the features of the Th-U cycle. Due to the relatively higher U isotope content in the LEU-started mode, the second peak of the radiotoxicity and decay heat of TRU and U appeared at about 10^5 years.

V. CONCLUSION

This work focuses on the optimization of the breeding capability of an MCFR and an investigation of the Th-U cycle performance based on an optimized MCFR. With the support of an in-house-developed optimization tool, the breeding capability of an MCFR at EQL was optimized. Based on the optimized MCFR, the B&B and PB&B scenarios have both been researched and discussed. Some important parameters, including heavy nuclide evolution, net ^{233}U production, TCR, and β_{eff} have been investigated to analyze the transition behavior of the optimized MCFR during whole operation. It can be concluded that in the B&B scenario, the Th-U cycle can be achieved with the average net ^{233}U production rate at EQL of 274 kg/a. Nevertheless, during the whole operation the maximum deficit of ^{233}U for the LEU-started, Pu-started, and TRU-started modes is 102, 87, and 83 kg, respectively. The fact that there is no available ^{233}U in nature exacerbates the problem. In addition, the TCR is always below −8.5 during the whole operation, which ensures safety during the whole operation. Moreover, it should be pointed out that for the LEU-started case, the value of β_{eff} decreased by 377 pcm during the whole operation, which needs to be noticed.

The PB&B scenario can solve the problem of ^{233}U deficiency in the B&B model well, and the ^{233}U production efficiency in the PB&B scenario is significantly higher. Nevertheless, the utilization efficiency of Th is relatively lower in the PB&B mode due to the online feeding of LEU/Pu. In the PB&B mode, with the ^{233}Pa extracted rate

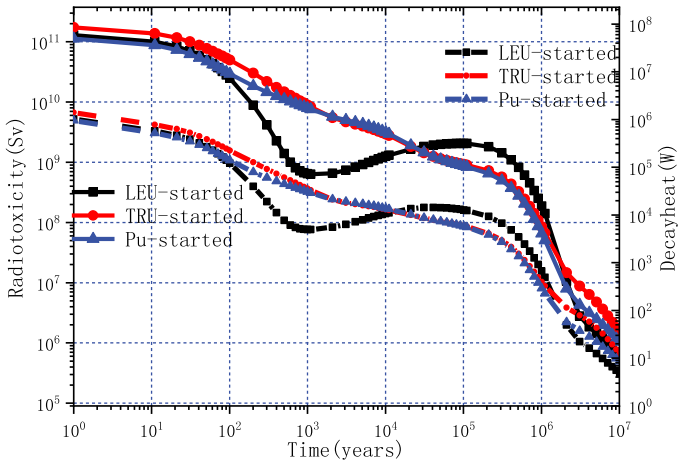

Fig. 23. Evolution of radiotoxicity and decay heat in EQL.

of 40 L/day, the net ^{233}U production rate is 570 kg/a and the corresponding DT is about 9.6 years in the three modes. While with a fast ^{233}Pa extracted rate, the LEU-started mode cannot always maintain criticality during the whole operation. When the core reprocessing rate increases to 200 L/day, the average net production of ^{233}U will increase to 807 and 803 kg/a, and the corresponding DT will decrease to 6.8 years in the TRU-started and Pu-started modes. Besides, the radiotoxicity and decay heat derived from the material losses in the LEU-started mode is higher than in the TRU-started and Pu-started modes due to the higher content of FPs, while the radiotoxicity and decay heat in the core is highest in the TRU-started mode thanks to the higher content of TRU. Thus, it is more suitable to use TRU or Pu as the starting and refueling materials in the PB&B mode due to the better ^{233}U breeding capability, which is helpful for the rapid production of ^{233}U and a rapid deployment of the Th-U cycle reactor.

Acknowledgments

This work is supported by the Chinese TMSR Strategic Pioneer Science and Technology Project under grant number XDA02010000, the National Natural Science Foundation of China under grant number 91326201, and the Shanghai nNatural under grant number 19ZR1468000.

References

1. "A Technology Roadmap for Generation IV Nuclear Energy System," Nuclear Energy Research Advisory Committee and the Generation IV International Forum, 2002: GIF-002-00, U.S. Department of Energy (2002).
2. J. SERP et al., "The Molten Salt Reactor (MSR) in Generation IV: Overview and Perspectives," *Prog. Nucl. Energy*, **77**, 308 (2014); https://doi.org/10.1016/j.pnucene.2014.02.014.
3. D. HEUER et al., "Towards the Thorium Fuel Cycle with Molten Salt Fast Reactors," *Ann. Nucl. Energy*, **64**, 421 (2014); https://doi.org/10.1016/j.anucene.2013.08.002.
4. M. KOSHI et al., "Self-Sustaining Core Design for 200 MWe Molten-Salt Reactor with Thorium-Uranium Fuel: Fuji-u3-(0)," *International Workshop on Thorium Utilization for Sustainable Development of Nuclear Energy* (TU2007), Beijing, China: Tsinghua University, 2007, December 4-6. (2007).
5. C. W. FORSBERG et al., "Design Options for the Advanced High-Temperature Reactor," *International Conference on Advances in Nuclear Power Plants, ICAPP* 2008. California, USA (2008).
6. C. Y. ZOU et al., "Optimization of Temperature Coefficient and Breeding Ratio for a Graphite Moderated Molten Salt Reactor," *Nucl. Eng. Des.*, **281**, 114 (2015); https://doi.org/10.1016/j.nucengdes.2014.11.022.
7. J. J. BULMER et al., "Reactor Design and Feasibility Study: Fused Salt Fast Breeder," Oak Ridge School of Reactor Technology, Oak Ridge, Tennessee (1956).
8. J. SMITH et al., "An Assessment of a 2500 MWe Molten Chloride Salt Fast Reactor," United Kingdom Atomic Energy Authority Reactor Group, Winfrith (1974).
9. A. MOUROGOV et al., "Potentialities of the Fast Spectrum Molten Salt Reactor Concept: REBUS-3700," *Energy Convers. Manage.*, **47**, *17*, 2761 (2006); https://doi.org/10.1016/j.enconman.2006.02.013.
10. I. SCOTT et al., "Stable Salt Reactor Design Concept," *Proc. Int. Thorium Energy Conf. Gateway to Thorium Energy*, Geneva, Switzerland, October 27-31, 2013 (2015).
11. A. HUKE et al., "The Dual Fluid Reactor—A Novel Concept for a Fast Nuclear Reactor of High Efficiency," *Ann. Nucl. Energy*, **80**, 225 (2015); https://doi.org/10.1016/j.anucene.2015.02.016.
12. M. H. JIANG et al., "Advanced Fission Energy Program—TMSR Nuclear Energy System," *Bull. Chin. Acad. Sci.*, **27**, 366 (2012); https://doi.org/10.3969/j..1000-3045.2012.03.016 (in Chinese).
13. C. G. YU et al., "Minor Actinide Incineration and Th-U Breeding in a Small FLiNaK Molten Salt Fast Reactor," *Ann. Nucl. Energy*, **99**, 335 (2017); https://doi.org/10.1016/j.anucene.2010.09.024.
14. G. C. LI et al., "Influences of Li-7 Enrichment on Th-U Fuel Breeding for an Improved Molten Salt Fast Reactor (IMSFR)," *Nucl. Sci. Tech.*, **28**, *7*, 97 (2017); https://doi.org/10.1007/s41365-017-0250-7.
15. G. C. LI et al., "Optimization of Th-U Fuel Breeding Based on a Single-Fluid Double-Zone Thorium Molten Salt Reactor," *Prog. Nucl. Energy*, **108**, 144 (2018); https://doi.org/10.1016/j.pnucene.2018.04.017.
16. C. Y. ZOU et al., "Transition to Thorium Fuel Cycle in a Small Modular Molten Salt Reactor Based on a Batch Reprocessing Mode," *Ann. Nucl. Energy*, **138**, 107163 (2019); https://doi.org/10.1016/j.anucene.2019.107163.
17. L. Y. HE et al., "Th-U Cycle Performance Analysis Based on Molten Chloride Salt Fast Reactor and Molten Fluoride Salt Fast Reactor," *Nucl. Sci. Tech.*, **31**, *83* (2020); https://doi.org/10.1007/s41365-020-00790-x
18. L. Y. HE et al., "Th-U and U-Pu Cycling Performances of Molten Chloride Salt Fast Reactor Under LEU Start-Up Mode," *Nucl. Tech.*, **43**, *1*, 10604 (2020); https://doi.org/10.11889/j.0253-3219.2020.hjs.43.010604 (in Chinese).

19. L. Y. HE et al., "Effect of ^{37}Cl Enrichment on Neutrons in a Molten Chloride Salt Fast Reactor," *Nucl. Sci. Tech.*, **31**, 27 (2020); https://doi.org/10.1007/s41365-020-0740-x.

20. L. Y. HE et al., "Research on the Optimization of Advanced High-Temperature Reactor Based on Hybrid Adaptive Genetic Annealing Algorithm," *Nucl. Power Eng.*, **40**, *5*, 56 (2019) (in Chinese).

21. D. Y. CUI et al., "Possible Scenarios for the Transition to Thorium Fuel Cycle in Molten Salt Reactor by Using Enriched Uranium," *Prog. Nucl. Energy*, **104**, 75 (2017); https://doi.org/10.1016/j.pnucene.2017.09.003.

22. F. CARLO et al., "Modelling and Analysis of the MSFR Transient Behavior," *Ann. Nucl. Energy*, **64**, *2*, 485 (2013); https://doi.org/10.1016/j.anucene.2013.08.003.

23. C. FIORINA et al., "Investigation of the MSFR Core Physics and Fuel Cycle Characteristics," *Prog. Nucl. Energy*, **68**, 153 (2013); https://doi.org/10.1016/j.pnucene.2013.06.006.

24. "SCALE: A Modular Code System for Performing Standardized Computer Analyses for Licensing Evaluations," ORNL/TM-2005/39, Version6.1, Oak Ridge National Laboratory (2009).

25. S. P. XIA et al., "Development of a Molten Salt Reactor Specific Depletion Code MODEC," *Ann. Nucl. Energy*, **124**, *2*, 88 (2019); https://doi.org/10.1016/j.anucene.2018.09.032.

26. G. C. LI et al., "Model Optimization and Analysis of Th-U Breeding Based on MSFR," *Nucl. Tech.*, **40**, 020603 (2017); https://doi.org/10.11889/j.0253-3219.2017.hjs.40.020603 (in Chinese).

27. E. H. OTTEWITTE, "Cursory First Look at the Molten Chloride Fast Reactor as an Alternative to the Conventional BATR Concept," Idaho National Engineering Laboratory (1992).

28. S. P. XIA, "Research on the High-precision Burnup Calculation Methods and Thorium-Uranium Fuel Breeding for the Liquid-Fueled Molten Salt Reactors," University of Chinese Academy of Sciences (2019).

29. E. MERLE-LUCOTTE et al., "Fast Thorium Molten Salt Reactors Started with plutonium," International Congress on Advances in Nuclear Power Plants (2006).

30. W. S. YANG, "Trends in Transmutation Performance and Safety Parameters Versus TRU Conversion Ratio of Sodium-Cooled Fast Reactors," *Proc. IEMPT-10*, Mito, Japan, October 6-10 (2008).

31. E. I. VAPIREV et al., "Conversion of High Enriched Uranium in Thorium-232-based Oxide Fuel for Light and Heavy Water Reactors: MOX-T Fuel," *Nucl. Eng. Des.*, **167**, *2*, 105 (1996); https://doi.org/10.1016/S0029-5493(96)01285-X.

32. D. Y. CUI et al., "Transition Toward Thorium Fuel Cycle in a Molten Salt Reactor by Using Plutonium," *Nucl. Sci. Technol.*, **28**, *10* (2017); https://doi.org/10.1007/s41365-017-0303-y.

33. M. AUFIERO, *Development of Advanced Simulation Tools for Circulating Fuel Nuclear Reactors*, PhD Thesis, University of California, Berkeley (2014).

34. "Energy Agency, Accelerator-driven Systems (ADS) and Fast Reactors (FR) in Advanced Nuclear Fuel Cycles," Technical Report, NEA-3109, U.S. Nuclear Energy Agency (2002).

35. H. J. PARK et al., "An Improved DeCART Library Generation Procedure with Explicit Resonance Interference Using Continuous Energy Monte Carlo Calculation," *Ann. Nucl. Energy*, **105**, 95 (2017); https://doi.org/10.1016/j.anucene.2017.03.012.